JOURNAL OF BACTERIOLOGY, Jan. 1991, p. 130–140
0021-9193/91/010130-11$02.00/0

Vol. 173, No. 1

Ultrastructure, Inferred Porosity, and Gram-Staining Character of *Methanospirillum hungatei* Filament Termini Describe a Unique Cell Permeability for This Archaeobacterium

TERRY J. BEVERIDGE,[1]* G. DENNIS SPROTT,[2] AND PAT WHIPPEY[3]

Department of Microbiology, College of Biological Science, University of Guelph, Guelph, Ontario, Canada N1G 2W1[1]; Division of Biological Sciences, National Research Council of Canada, Ottawa, Ontario, Canada K1A 0R6[2]; and Department of Physics, University of Western Ontario, London, Ontario, Canada N6A 3K7[3]

Received 27 July 1990/Accepted 18 October 1990

By light microscopy, *Methanospirillum hungatei* GP1 stains gram positive at the terminal ends of each multicellular filament and gram negative at all regions in between. This phenomenon was studied further by electron microscopy and energy-dispersive X-ray spectroscopy of Gram-stained cells, using a platinum compound to replace Gram's iodine (J. A. Davies, G. K. Anderson, T. J. Beveridge, and H. C. Clark, J. Bacteriol. 156:837–845, 1983). Crystal violet-platinum precipitates could be found only in the terminal cells of each filament, which suggested that the multilamellar plugs at the filament ends were involved with stain penetration. When sheaths were isolated by sodium dodecyl sulfate-dithiothreitol treatment, the end plugs could be ejected and their layers could be separated from one another by 0.1 M NaOH treatment. Each plug consisted of at least three individual layers; two were particulate and possessed 14.0-nm particles hexagonally arranged on their surfaces with a spacing of a = b = 18.0 nm, whereas the other was a netting of 12.5-nm holes with spacings and symmetry identical to those of the particulate layers. Optical diffraction and computer image reconstruction were used to clarify the structures of each layer in an intact plug and to provide a high-resolution image of their interdigitated structures. The holes through this composite were three to six times larger than those through the sheath. Accordingly, we propose that the terminal plugs of *M. hungatei* allow the access of larger solutes than does the sheath and that this is the reason why the end cells of each filament stain gram positive whereas more internal cells are gram negative. Intuitively, since the cell spacers which partition the cells from one another along the filament contain plugs identical in structure to terminal plugs, the diffusion of large solutes for these cells would be unidirectional along the filament-cell axis.

The Gram stain has traditionally been used by microbiologists as a preliminary method for determining shape, size, and intactness of bacteria by light microscopy. In eubacteria, since the staining mechanism is a relatively good measure of general wall structure, chemistry, and integrity (2, 3, 10, 16), it can also be used in a taxonomic way to divide these cells into gram-negative, gram-positive, and gram-variable varieties. Those cells with a high lipid compared with peptidoglycan content in their walls are usually gram negative, whereas if the reverse is true, they are gram positive (3, 16). Gram variability is also dependent on the type of cell wall (2). The development of a Gram staining regimen using an aqueous potassium trichloro-(η^2-ethylene)-platinum(II) (or potassium TPt) solution to replace Gram's iodine has greatly facilitated elucidation of the Gram reaction. This platinum compound (TPt) complexes with crystal violet via a metathetical anion exchange, forming a more neutral charge transfer complex with the pi bonds of the dye and precipitates from solution. In a chromographic manner, this resembles the crystal violet-iodide complex of the traditional Gram stain which is responsible for gram positivity (10). Since it contains platinum as a stable electron-dense agent, it can be used for electron microscopy and can be identified by energy-dispersive X-ray spectroscopy (EDS) (3, 10).

Compared with eubacteria, archaeobacteria have very unusual enveloping structures (13). For example, they can possess multilayered surfaces (e.g., *Methanosaeta* (*Methanothrix*) spp. [5]), pseudomurein-containing walls (e.g., *Methanobacterium* spp. [14]), single S layers (e.g., *Methanococcus* spp. [12]), or no wall layers at all (e.g., *Thermoplasma* spp. [21]). They are frequently Gram stained when looked at by light microscopy and are distinguished from one another by their stainability. Yet there has been no research on this group of bacteria to accurately present a mechanistic view of their staining response.

Methanospirillum hungatei has one of the most complex envelopes of all archaeobacteria (13) and grows naturally as linear chains of cells (up to 9 to 12 cells long; Fig. 1 and 2), all confined within a paracrystalline sheath (17) as the outermost boundary layer. Proteinaceous particles, possessing cross-beta structure, occupy a 5.6- by 2.8-nm unit cell, are arranged with p2 symmetry on the surface of larger hooplike structures, and are surrounded by narrow holes which appear to penetrate the sheath (7, 20). Plugs which are multilamellar partitions are found along the filament at cell spacers as well as at filament ends (4); they, like the sheath, are paracrystalline, but they possess a larger subunit spacing and p6 symmetry (17). Cells of *M. hungatei* are unique because, in addition to their walls, they are surrounded by a sheath in their longitudinal dimension and plugs at their polar ends (Fig. 1). Since the Gram response in eubacteria is a reflection of the cell-enveloping structures, it was of interest to study this complex bacterium by electron microscopy and EDS using the TPt-modified Gram stain.

* Corresponding author.

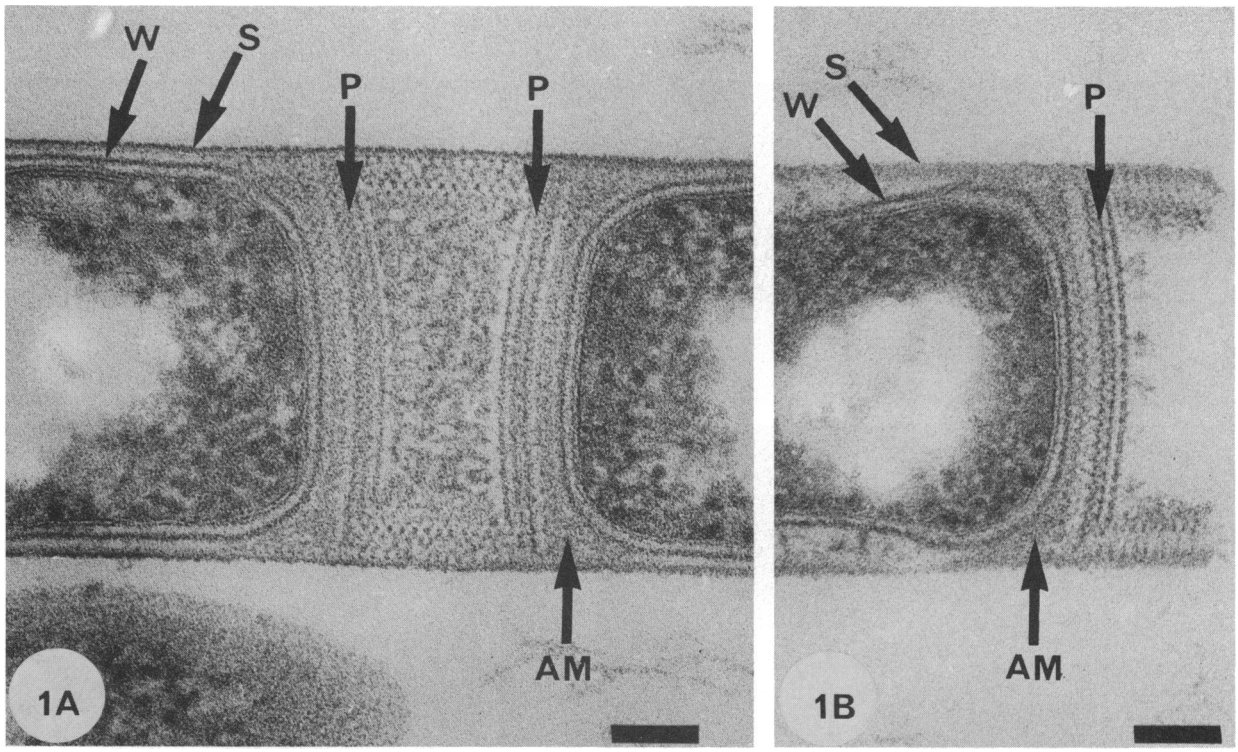

FIG. 1. Thin-section composite showing cell spacer plugs (A) and an end plug (B). P, Plug; S, sheath; W, cell wall; AM, amorphous matrix. Bars = 100 nm.

MATERIALS AND METHODS

Culture growth. Long filaments of *M. hungatei* GP1 were induced by growth as either static cultures or slowly agitated cultures (20 rpm on a rotary platform) in 100 ml of modified SA medium containing acetate (15) to exponential growth phase (optical density at 600 nm of 0.5 [path length, 1 cm]) in sealed 1-liter pressure bottles under a positive atmosphere of 4 H_2/1 CO_2 (vol/vol) at 37°C (15). Samples were removed as needed for light or electron microscopy by using a syringe, relying on the positive pressure within the growth vessels to maintain anaerobiosis.

Gram stain, light microscopy, electron microscopy, and EDS. Stains for light microscopy were done on heat-fixed cells of *M. hungatei* when growth had attained an optical density at 600 nm of 0.5. A drop of cells was placed on a glass slide, smeared over the surface, and gently heated until dry. Crystal violet flooded the smear for 60 s, followed by an equal volume of Gram's iodine solution (conventional Gram stain) or an aqueous 50 mM potassium TPt solution (TPt-modified procedure) for an additional 60 s. The smears were gently washed under running tap water (~4°C) and blotted dry with absorbent filter paper. They were then decolorized under a slow, steady stream of hydrous 95% ethanol for 30 s, washed with water, blotted dry, and counterstained with carbol fuchsin for 60 s. For some experiments, the staining and decolorization times were increased to 120 s. The smears were washed with water, blotted dry, and observed by light microscopy, using a Zeiss Photomicroscope (Universal model; Carl Zeiss, Oberkochen, Federal Republic of Germany). Both bright-field and phase microscopy required a 100/1.25 oil immersion apochromatic objective lens. Images were recorded on T-Max black-and-white film developed in D-76 (Eastman Kodak, Rochester, N.Y.) and were printed onto Kodabromide F4s paper (Eastman Kodak). Under these conditions, the gram-positive ends of filaments were black whereas the gram-negative regions were light gray (Fig. 3).

For electron microscopy and EDS, cells were harvested by centrifugation and washed twice in 50 ml of 50 mM HEPES (*N*-2-hydroxyethylpiperazine-*N'*-2-ethanesulfonic acid) buffer at pH 6.8 containing 1 mM $MgCl_2$. They were then put through either the conventional or TPt-modified Gram procedure as outlined above. More detail can be found in Fig. 1 of Davies et al. (10). They were then equilibrated back to 50 mM HEPES buffer, fixed for 1 h in 5% (vol/vol) glutaraldehyde in buffer, washed (without heavy-metal staining), and processed into Durcupan (Fluka AG, Buchs SF, Switzerland) or Epon 812 (CanEM, Guelph, Ontario, Canada). From previous experience, Durcupan best preserves the TPt-crystal violet complex but is difficult to contrast with uranyl and lead once sectioned. For this reason, Durcupan was used most frequently for EDS analysis, whereas Epon was used for electron microscopy.

EDS was performed on unstained thin sections, using the X-ray spectrum from the embedding resin as an index of specimen background radiation. Pt ($M_{\alpha,\beta}$ and $L_{\alpha,\beta}$) lines were monitored for the Gram precipitate (the TPt-crystal violet complex). Spectral lines slightly upstream and downstream in the X-ray spectrum were used to establish readings of the continuum to ensure the validity of the Pt readings. Point analyses were performed on a Philips EM400T equipped with a scanning transmission electron microscope (STEM) module and an EDAX/9100/40 EDS system at 100

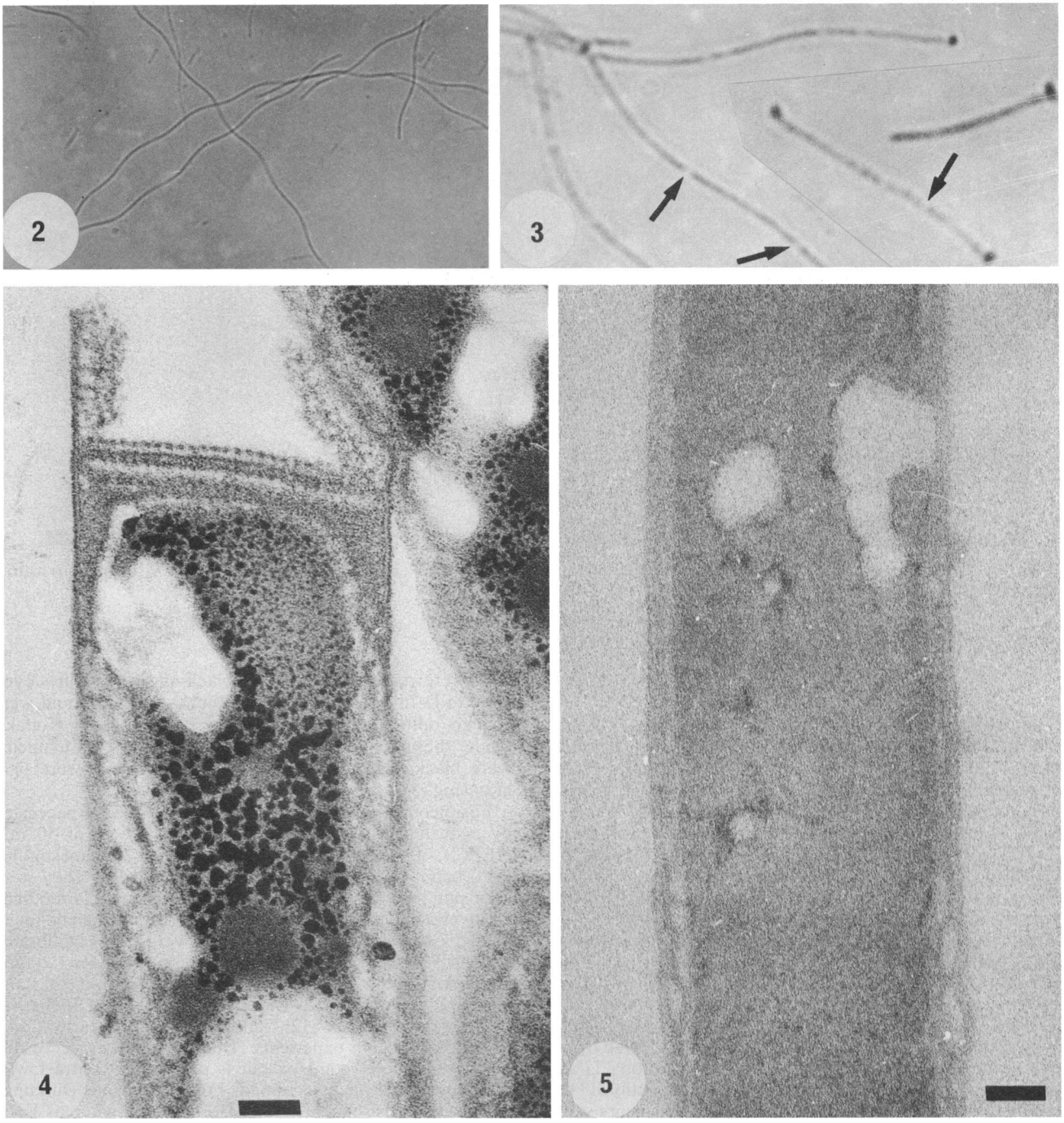

FIG. 2. Phase (light) micrograph of the filaments photographed directly from the culture used for Gram staining in Fig. 3 to 5.

FIG. 3. Bright-field (light) micrographs of both long and short filaments after Gram staining. The filament ends are dark (gram positive) because of the purple color of the crystal violet. The remainder of the filaments is gram negative. Areas of very light intensity could correspond to cell spacer regions (some are marked with arrows). In both Fig. 2 and 3, the filament diameters are 500 nm.

FIG. 4. Thin section of a portion of a terminal cell in a filament Gram stained by the TPt method. The end plug is toward the top of the figure. The dark cytoplasmic precipitates are TPt-crystal violet complexes (as identified by a strong EDS Pt signal), which make this cell gram positive. The cells tangentially sectioned to the right of this cell are also filled with stain and must be terminal cells. Bar = 100 nm.

FIG. 5. Thin section of the middle cell of a seven-cell-containing filament. No precipitates were seen, and no Pt was identified by EDS. Bar = 100 nm.

kV, using a spot size of 200 nm and an emission current of 80 μA. Typically, magnifications of ×280,000 and counting times of 100 to 200 s were used. When Pt distribution maps were necessary, the STEM mode was used and the microscope was operated at 80 kV and 85 μA with a 50-μm condenser aperture in place. Typical magnifications in this mode were ×37,000 with scan times of 500 s.

Once unstained sections had been used for EDS, they were then counterstained with uranyl acetate and lead citrate (3, 10) to increase contrast and to ensure the proper identification of cellular constituents. Pt could still be identified on these stained cells although there was overlap of the Pt and Pb lines (both L and M lines). Images were recorded by either a Philips EM400T or EM300 transmission electron microscope operating under standard conditions with liquid nitrogen cold traps in place.

Preparation of plugs for optical diffraction and computer enhancement of image. *M. hungatei* was transformed to spheroplasts in 16.2 mM dithiothreitol at pH 10 and subjected to osmotic lysis and discontinuous sucrose gradient centrifugation (19). After centrifugation at 110,000 × *g* for 22 h, the sheath banded at the 65 to 70% (wt/vol) sucrose region and, after dialysis against water to remove sucrose, was treated with 1% sodium dodecyl sulfate (SDS) at 90°C for 30 min to remove contaminating cellular material. SDS was removed by washing in water; the material was then treated with 0.1 M NaOH for 60 min at 23°C to remove the plugs from the sheath material. Centrifugation at 10,800 × *g* for 10 min removed most intact sheaths from suspension and left the plugs in the fluid phase. These were centrifuged at 40,000 × *g*, the pellets were resuspended in water, and intact plugs were negatively stained for electron microscopy in 1% uranyl acetate. Further treatment of intact plugs in 0.1 M NaOH for 60 min at 23°C disrupted the bonding forces that held together the individual layers of each plug. Surface tensional forces during drying of 2% uranyl acetate negative stains of the material were frequently strong enough to separate the layers.

Platinum shadows of plugs were produced in a Balzers BA360M freeze-etcher at a shadowing angle of 30° and a vacuum of 126 kPa.

Optical diffraction of images of negatively stained intact and separated plugs was used to ensure suitable defocus levels, coherent diffraction maxima, lattice arrangements, and subunit spacings. The 2.8-nm repeat of the sheath (20) was used as an internal calibration standard. Twenty separate images of each variety of plug or plate were analyzed by optical diffraction to ensure consistency, and suitable select images were chosen for image enhancement processing.

These images were digitized on a 50-μm raster by using an Optronics drum scanner. The resulting digital 8-bit images were processed by using a set of programs written in Fortran on a PDP 11-44 computer. A typical image-processing sequence involves masking off the area of interest, scaling the image so that the useful information is stored in the range 0 to 255, and taking the Fourier transform. The resulting pattern was observed on a television monitor with the pixels in the Fourier transform set to zero, except in the vicinity of the lattice vectors. The inverse transform was then calculated to obtain the enhanced image.

Sheared filament ends for orientation studies. Sheath cylinders were prepared by the dithiothreitol-SDS method described above. The sheath-plug preparation was sheared by passing it through a Potter-Elvehjem tissue homogenizer 20 to 30 times, which broke the sheath apart in several places along its length, some of which contained plugs. This preparation was Pt shadowed as previously described, and the topography of the plate surfaces was used for orientation.

RESULTS AND DISCUSSION

General cell morphology and Gram staining. Cells of *M. hungatei* are enclosed by two different physical structures, sheaths and plugs, when they are encased within a multicellular filament (Fig. 1). Thin sections showed cell spacer plugs and terminal plugs (4) to be similar multilaminar structures; each consisted of at least three electron-dense layers (cf. Fig. 1A and B) which were attached to the sheath and which separated the cells from one another (cell spacer plugs) and from the external milieu (terminal plugs). The sheath was a continuous cylinder that enclosed the chain of cells along the periphery of their longitudinal axis (Fig. 1; 4).

Under our growth conditions, filaments with a long, shallow, spiral axis which contained chains of 2 to 10 cells predominated the culture (Fig. 2). The filaments were motile (most frequently those filaments of two to five cells) by means of flagella extending from their termini (18), emphasizing the vitality of the end cells. When Gram stained, only the ends of each filament became gram positive, and this was apparent on both long and short filaments (Fig. 3). The remaining regions between the ends stained gram negative. Careful scrutiny of these gram-negative regions revealed areas of light stain intensity which presumably corresponded to the cell spacers between cells. Given this visual index of cell length, it was apparent that most of the gram positivity associated with end cells occurred at their termini (Fig. 3).

Electron microscopy of filaments Gram stained by the TPt method revealed a distinct preponderance of electron-dense precipitates in the end cells of each filament. EDS identified Pt as a major constituent in the precipitates; this was the crystal violet-TPt complex which was responsible for gram positivity. The complex dominated the terminal portion of the end cells in each filament (Fig. 4) and was rarely, if ever, seen in cells toward the middle (Fig. 5). In fact, when EDS was performed along the length of filaments, the Pt signal became weaker as the distance away from the termini progressed (Table 1). The reverse situation was true for P, which is a natural cellular constituent (phospholipids, nucleic acids, etc.). The termini of control filaments that were not Gram stained retained a strong P signal.

These observations suggested that the migration of the

TABLE 1. Distribution of the crystal violet-TPt complex along a *M. hungatei* filament containing seven cells[a]

Filament part	% Wt of element		
	Pt(L)	P(K)	Cl(K)
Ends	65	7	31
Second cells from ends	38	33	32
Middle cell	0	60	37

[a] Although the data are for the analysis of one filament, they are representative of data for 16 filaments that were analyzed. Since each filament has two ends and two second cells from ends, the values are averages of these readings for one filament and are consistent to ±2 to 4%. The data were produced by EDS analysis of thin sections and are expressed as the percent weight ratio after background radiation has been subtracted. For Pt, the $L_{\alpha,\beta}$ lines were used; for P and Cl, the $K_{\alpha,\beta}$ lines were monitored; the Pt signal is from the crystal violet-TPt precipitate, the P is an index of cellular components such as nucleic acids and phospholipids, and the Cl is a natural constituent of the plastic used to infiltrate cells, although it is also a natural but highly diffusible cellular anion. The constant Cl signal ensures proper plastic infiltration of the filament.

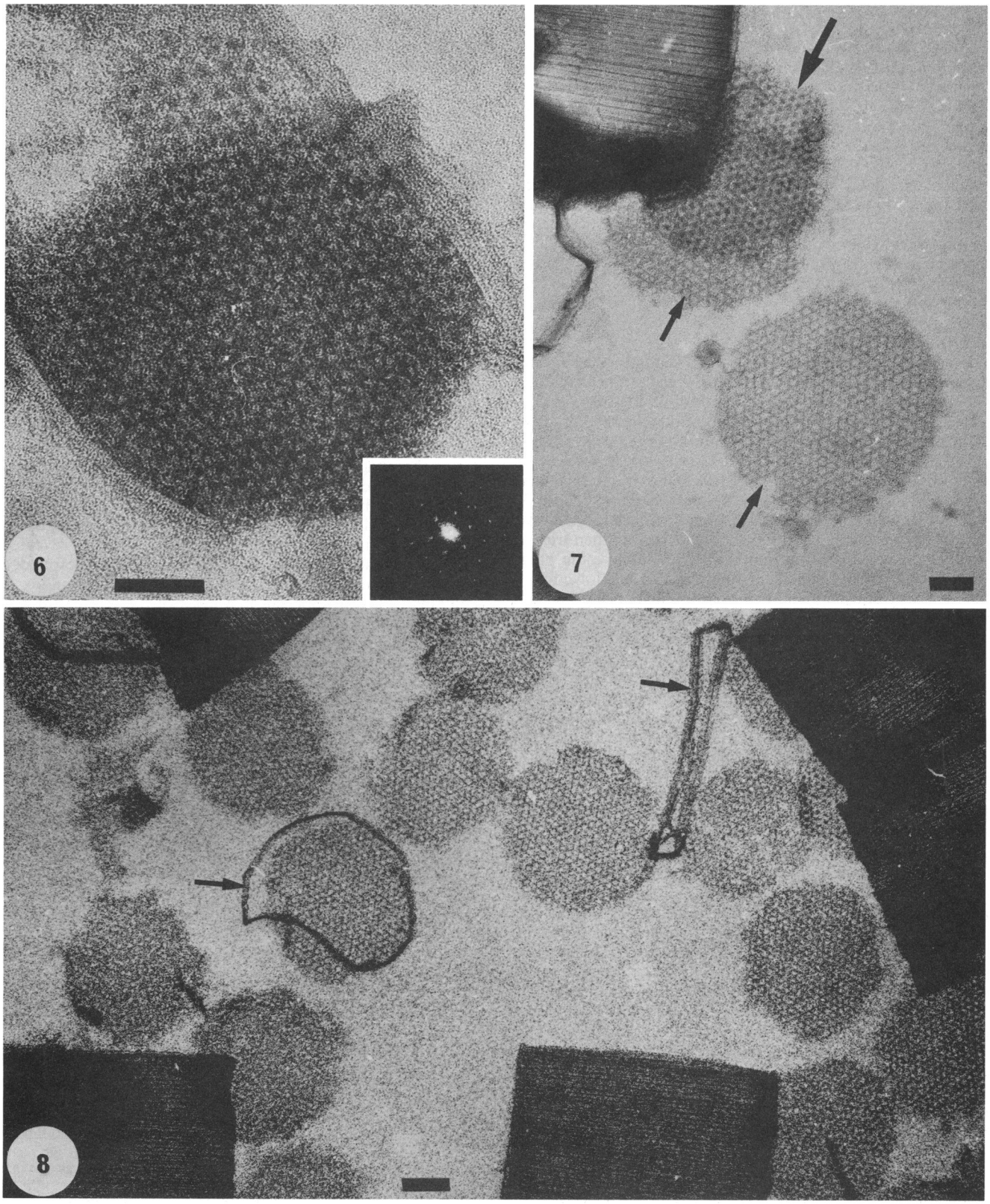

FIG. 6. Negatively stained (2% uranyl acetate) intact plug showing a moiré of interdigitated structure. The inset shows its optical transform. Thin sections of intact plugs showed them to be made up of the same structural layers as was seen in intact (Fig. 1) and spheroplasted (Fig. 9) cells. Bar = 100 nm.

FIG. 7. Negative stain of the three plates of a plug which are dissociating themselves from one another and the sheath after 0.1 M NaOH treatment. Notice that two plates are particulate (small arrows) and that one is a netting of holes (large arrow). Bar = 100 nm.

FIG. 8. Negative stain of the preparation used to do structural analysis. The plates are highly enriched compared with the sheath and their constituent hoops (arrows). Bar = 200 nm.

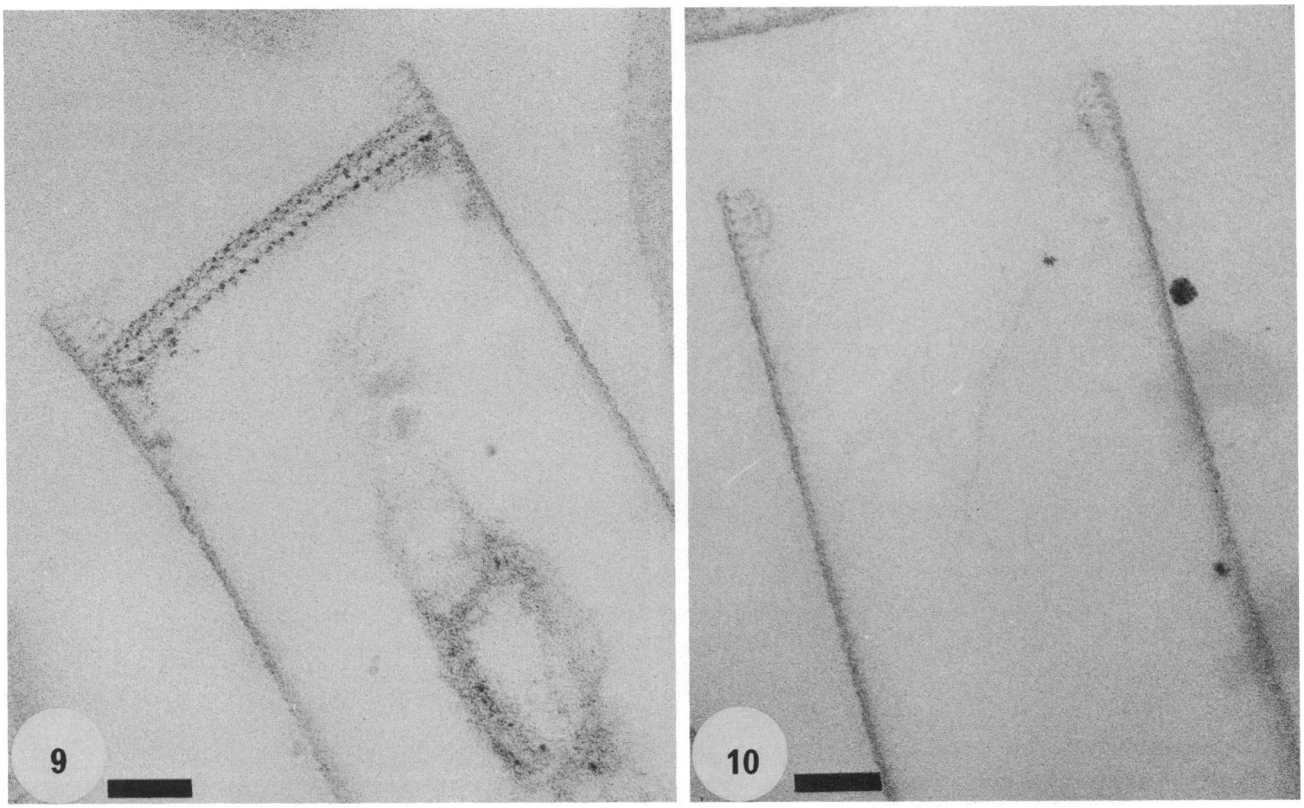

FIG. 9 and 10. Thin sections showing the terminal ends of a sheath before 0.1 M NaOH treatment (Fig. 9; the three plates of a plug are seen) and after treatment (Fig. 10), showing that the plates are removed. Bars = 100 nm.

stain and the cellular constituents occurred along the filament axis. As crystal violet, TPt, or ethanol (decolorizing agent) penetrated along from the ends of the filaments, small diffusible P-containing components were dissolved and eventually leached out. This seemed to be a time-dependent phenomenon that relied on diffusion, since stain buildup and cellular leaching occurred in a progressive sequence from filament end toward filament middle. Longer staining times increased the progression of the stain. These observations suggested that of the two enveloping structures (i.e., sheath and plug), it was the plugs that were permeable to the Gram reagents.

Structural analysis of plugs. Our structural analyses are in broad agreement with those of Shaw et al. (17); the plugs were circular and surprisingly uniform in size, having a diameter of ca. 0.45 μm, which approximated the diameter of the cells in the sheath (Fig. 1). Negatively stained intact plugs (Fig. 6) produced low-order reflections in optical transforms and suggested a hexagonal arrangement of subunits. High-order data such as seen in the insert of Fig. 6 were difficult to obtain consistently. Since thin sections revealed the existence of three separate plates or layers to each plug (Fig. 1 and 4), the difficulty of obtaining high-order reflections on transforms of intact plugs could be due to the shifting of the layer elements with respect to one another to form discordant moirés of superimposed particles.

Treatment with 0.1 M NaOH not only removed the plugs from the sheath but also caused the plate layers to separate from one another (Fig. 7) until the plates were spread throughout the suspension as discrete entities (Fig. 8). Thin-section analysis of the preparation before (Fig. 9) and after (Fig. 10) NaOH treatment confirmed that there was complete removal of the three plates. Thin sections of the plugs revealed each plate to possess a regular arrangement of holes (Fig. 9). Careful examination of negatively stained preparations during plug extrusion substantiated the existence of three layers per plug and revealed that two layers were of similar subunit arrangement, whereas the remaining layer possessed a different organization (Fig. 7); the latter structure was always found in smaller numbers than the former (Fig. 8).

These single layers could be negatively stained and imaged at high resolution. The most abundant type possessed a hexagonal arrangement of broadly circular 14-nm-diameter particles possessing an angular or faceted infrastructure around which the stain penetrated and pooled (Fig. 11). The other type of layer was a netting of hexagonally arranged, circular holes which were slightly smaller (13 nm) than the particles on the most abundant layer (Fig. 12). Images of both layers were amenable to optical diffraction and produced subtly different patterns to a limiting resolution of ca. 4.0 nm (insets of Fig. 11 and 12). It was possible that the act of separating the layers from one another had subtly perturbed macromolecular arrangements enough to inhibit higher resolution; the internal diffraction standard of the sheath consistently revealed the 2.8-nm repeat. Computer reconstructions of the images of each layer confirmed our initial analyses; one layer was composed of a hexagonal arrangement of circular 14.0-nm particles (Fig. 13). Each particle had six thin arms extending from it along its sixfold axes which separated the particles from one another, produced an intersubunit spacing of a = b = 18.0 nm, and gave

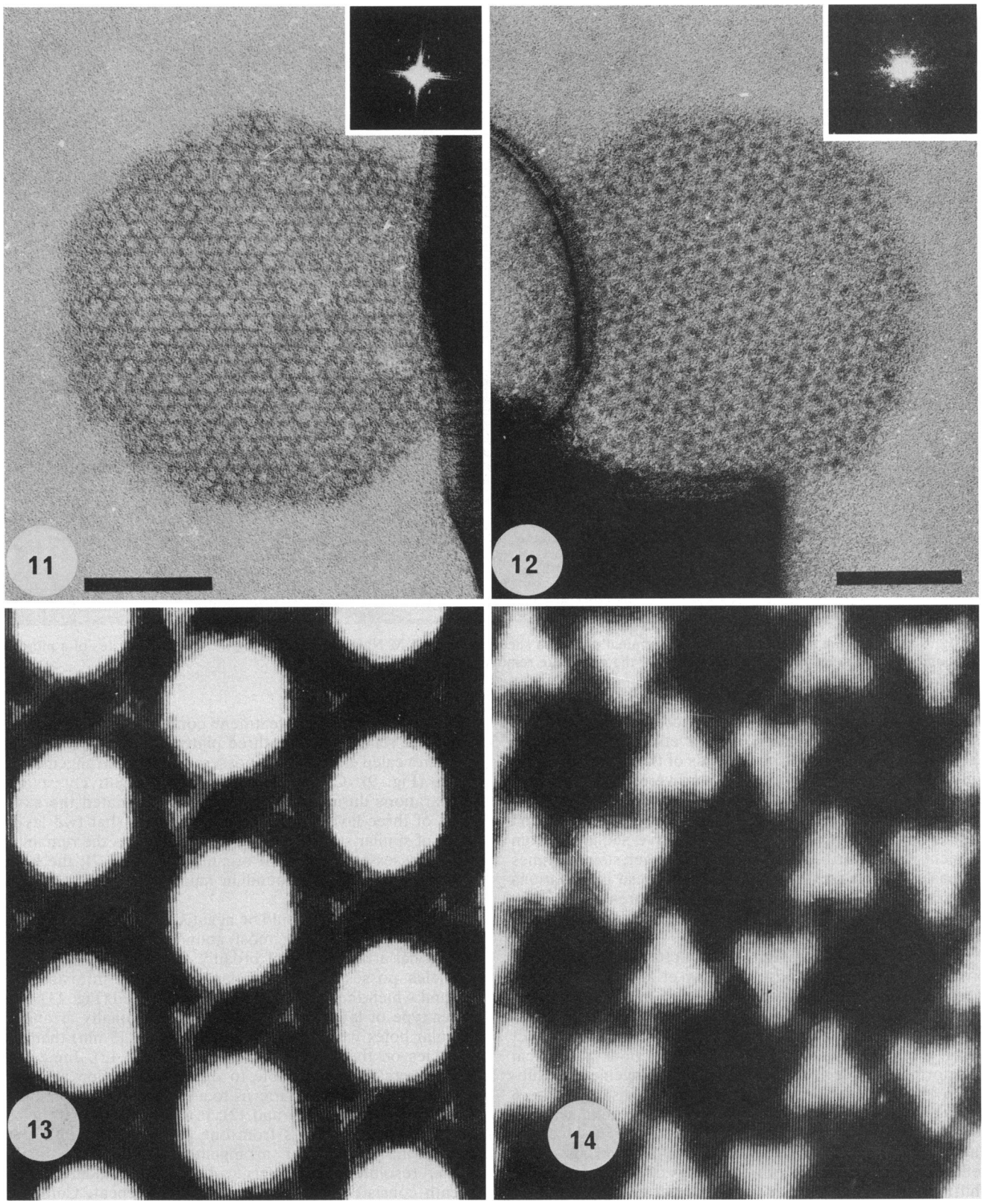

FIG. 11. High-resolution micrograph of the particulate layer and its optical transform. Bar = 100 nm.

FIG. 12. High-resolution micrograph of the holey layer and its optical transform. Bar = 100 nm.

FIG. 13. Computer reconstruction of the particulate layer at high magnification. The subunit particles are white, and the thin arms extending from each particle are gray. The holes are black. Center-to-center spacing = 18.0 nm.

FIG. 14. Computer reconstruction of the holey layer at high magnification. The subunit particles are delta-shaped units linked to one another by delicate gray linkers at each tip. The holes are black. Center-to-center spacing = 18.0 nm.

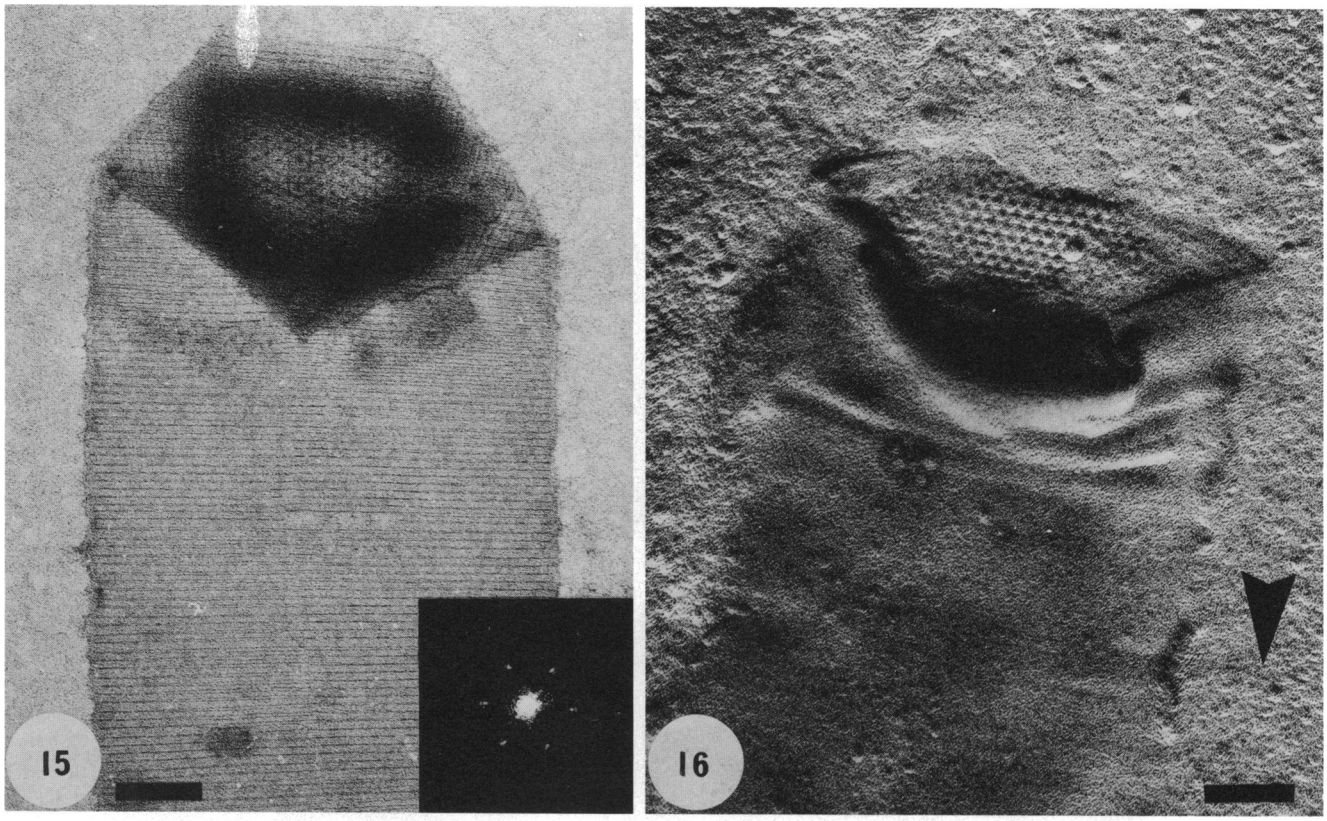

FIG. 15. Negative stain of a terminal plug at the end of a filament which shows the complex moiré that the plates produce. The inset is the optical transform and confirms the p6 alignment of elements. Bar = 100 nm.

FIG. 16. Pt-shadowed terminal plug at a filament end, showing the outermost plate of the plug to be particulate. Bar = 100 nm. In this and other shadowed preparations, the large arrow denotes shadow direction.

the subunits their angular faceted infrastructure. This spacing was almost identical to the spacing found by Shaw et al. for intact plugs (i.e., 18.2 nm [17]). The other layer also possessed p6 symmetry but was a network of holes 12.5 nm in diameter (Fig. 14). The subunit elements of this holey layer were trimeric in form and closely resembled those described by Shaw et al. in their description of the plug's subunit makeup (17). As in the particulate layer, a = b = 18.0 nm.

It was apparent that the holes between the particles in the particulate layer were shaped differently from those in the holey layer (cf. Fig. 13 and 14). Those of the holey layer were roughly circular, whereas those of the particulate layer were oblong (ca. 12.5 by 7.0 nm) and arranged along a sixfold axis around each particle.

Orientation of the plates within a plug. There are a number of possible ways in which the three plates of each plug could be stacked. For correct natural orientation, the plug must be positioned within the sheath. Negative stains of the ends of filaments revealed the natural position of the end plug, but the stain penetrated between and around the plates so as to produce moirés of superimposed elements (Fig. 15). Optical diffraction of these images gave no more than two orders of reflections but aptly demonstrated the p6 alignment of elements (inset, Fig. 15). These transforms also compared well with low-order reflections in Fig. 6, 11, and 12, which suggested that gross alteration of macromolecular detail affecting pore size had not occurred during 0.1 M NaOH treatment and plug extrusion. Thin sections showed that each plug rested on a lightly stained amorphous matrix which was positioned between the cell wall and the plug (Fig. 1 and 9). The particulate and holey plates of the plug could not easily be identified in these preparations, yet it seemed possible that the amorphous matrix, on the inside surface of each plug, could be used in other techniques to help identify the plug faces.

Pt shadowing is a topographical method and revealed the outermost plate of a terminal plug to be particulate (Fig. 16). Filaments denuded of cells as explained in Materials and Methods and broken by the shear forces generated by a Potter-Elvehjem tissue homogenizer produced cell spacer and terminal ends which could be identified by their retention of plugs. Pt shadows of this preparation revealed two plug topographies: the particulate surface (Fig. 17) and a smooth amorphous surface (partially obscuring the particulate surface) (Fig. 18). Intact plugs removed by 0.1 M NaOH treatment confirmed these topographies (Fig. 19 and 20). Since at no time was a holey layer seen in these shadowed preparations, we believe the smooth surface on some plugs to be the inner amorphous matrix seen in thin sections (Fig. 1). Accordingly, the plate orientation within plugs must be as is seen in Fig. 21: two particulate layers sandwich the holey layer.

Alignment of the plate holes within a plug. The identical p6 symmetries of each plate within a plug suggest that they are aligned in register to one another (e.g., as in Fig. 21). Thin

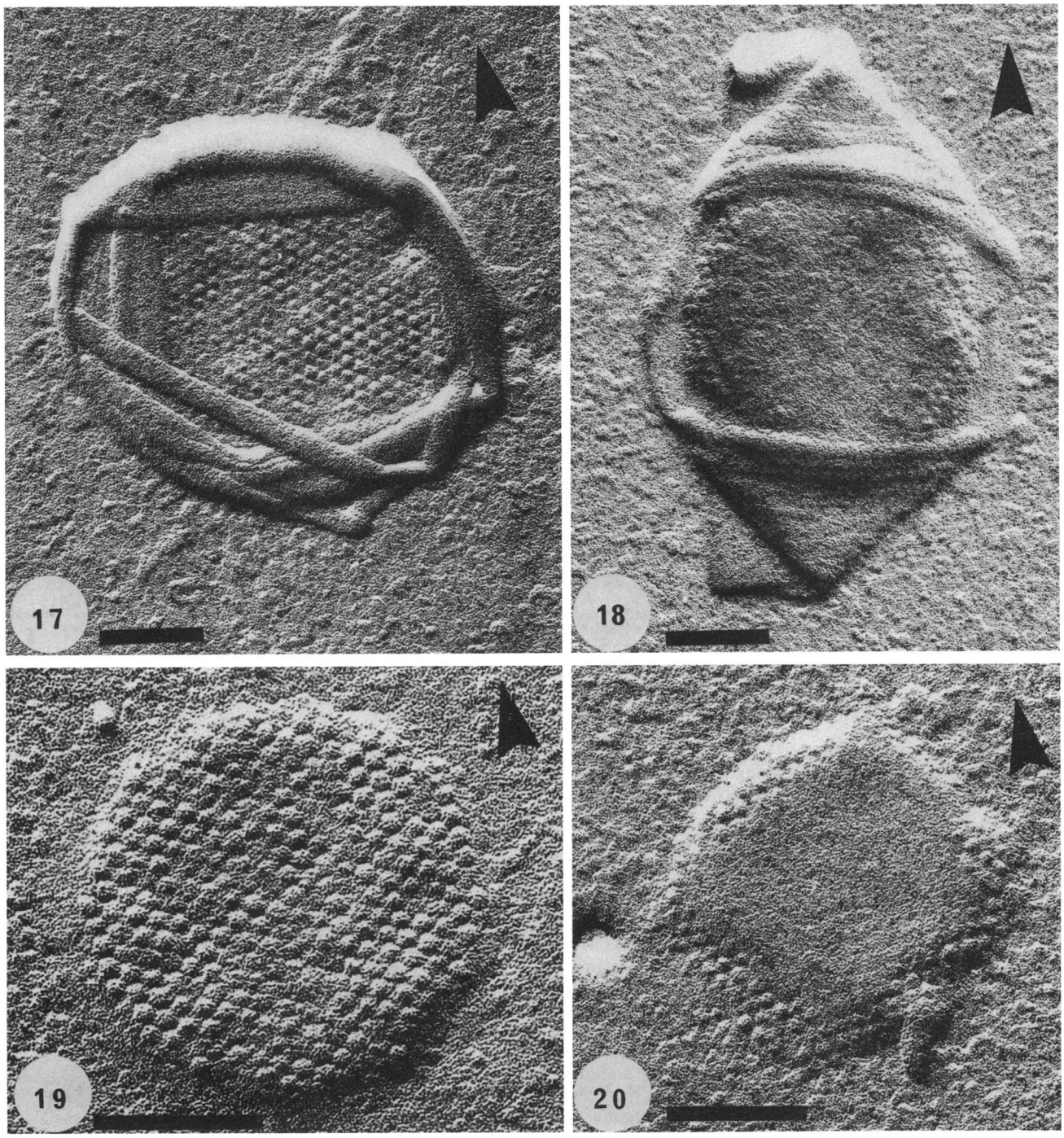

FIG. 17. Pt-shadowed terminal plug in a small sheared fragment of sheath, which confirms the outermost plate to be particulate. Bar = 100 nm.

FIG. 18. Pt-shadowed plug in a sheared sheath fragment showing the innermost surface, which is partially obscured by the amorphous matrix seen in Fig. 1. The innermost layer is also particulate. Bar = 100 nm.

FIG. 19 and 20. Pt-shadowed, intact plugs isolated by the 0.1 M NaOH method showing both outer (Fig. 19) and inner (Fig. 20) plates to be particulate. As in Fig. 18, the innermost surface in Fig. 20 is partially obscured by the amorphous matrix. Bar = 100 nm.

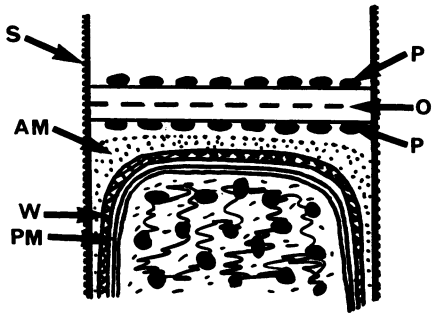

FIG. 21. Drawing to show the arrangement of the plates within a terminal plug and the plug's association with the other enveloping structures. The alignment of the plates with respect to one another is such that the particles obscure the holes of the middle netting layer (i.e., the first case described in the text). It is also possible that the particles could exist at half an interval removed from that which is drawn (i.e., the second case). The drawing is not to scale. S, Sheath; W, cell wall; PM, plasma membrane; AM, amorphous material; P, particulate layers of the plug; O, holey layer of the plug.

sections (e.g., Fig. 1A, 4, and 9) also suggested the plates to be in register with one another. The difficulty was to ascertain the exact alignment of this register. The two most logical alignments from the available data would be (i) to have the particles of the two particulate layers fitted adjacent to the actual fabric of the holey layer such that they lie against the nodes of the netting or (ii) to have the particles fitted into and partially occupying the holes of the holey layer (as shown in Fig. 21).

The first case, which aligns the holes in each plate, is the most permeable situation and is in accordance with the results of Shaw et al. (17). Yet at the time of the analyses of Shaw et al., the plug was considered most probably to be only a double layer of similar elements. They also did not account for the possibility, during their preparation for electron microscopy, that the three plates within the plugs could have shifted. We also cannot be certain of this. For this reason, we must consider the second case.

This case presumes some blockage of the holes and should be the least permeable of the two situations. It was important to determine the degree of blockage and relate it back to the Gram stain results, since it was possible that the staining reagents could be excluded by intact plugs.

Since the images of intact plugs (Fig. 6) produced only low-resolution transforms and since the plates in these plugs could be shifted, we resorted to computer manipulation of the individual plates to stack them into the blockage format. For simplicity, only one particulate layer was stacked together with one holey layer. We assume that the additional particulate layer would be aligned to the other plates along the same sixfold axes and that this alignment would produce the same porosity as in the two-plate situation; i.e., the three plates of an intact plug would have the same porosity as shown in our computer-simulated two-plate model. Figure 22 shows the model; it is apparent that even when the particles overlie the holes of the holey layer, there remains a substantial pore for solutes to pass through. The pores are similar in shape to those holes seen in the particulate layer and are approximately 80% of their size (cf. Fig. 13 and 22).

Consequences of plug porosity for Gram staining and the natural diffusion of solutes. The sheath of *M. hungatei* is a very resilient and nonporous structure; it is difficult to degrade (9), and it contains very small holes no more than

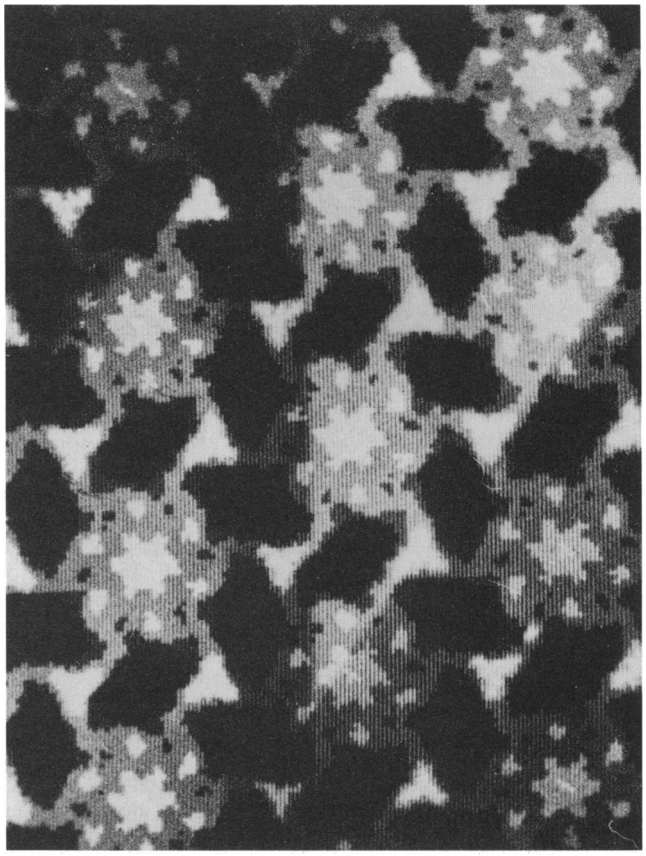

FIG. 22. Computer reconstruction of a two-plate composite when the particulate and holey layers are aligned as in the second case described in the text. The light regions are areas where the stain is excluded; the black areas are the holes. Center-to-center spacing = 18.0 nm.

2.0 nm in diameter (17, 20) which approximate the size of cellular substrates (H_2, CO_2, and NH_3) and end product (CH_4). The spacer and end plugs, on the other hand, consist of three plates. Two are particulate and have 12.5- by 7.0-nm holes permeating them, whereas the middle plate is a netting of larger and roughly circular 12.5-nm holes. As individual plates, each of these layers has a porosity greater than that of the sheath. If they are stacked together as in the first case, the holes of each plate are aligned and the two particulate layers would be the restricting layers with 12.5- by 7.0-nm pores. If they are stacked together as in the second case, the particles of the particulate layers fit in and plug up the large holes of the middle layer and the fabric of the middle layer partially obscures the holes in the particulate layer; these pores are reduced in size about 80% and become 12.0 by 6.0 nm. Either alignment ensures that the plugs are three to six times more porous than the sheath.

As a soluble cation, crystal violet resembles a three-bladed propeller about 1.88 nm in diameter and 0.65 nm thick (10). TPt forms a smaller ellipsoid anion about 0.82 by 0.62 nm in dimension, whereas I^- and I_3^-, which are used in the traditional stain, are small spheres of 0.43 and 0.60 nm, respectively (10). For the Gram stain, if crystal violet, TPt, and I^-/I_3^- are freely diffusible, each could penetrate the end plugs of a filament with no difficulty. Since crystal violet approaches the maximum diameter of the sheath pore, it

could be excluded. In addition, our evidence suggests that the sheath pore is electronegatively charged as a result of carboxylates (6). It is likely that crystal violet, being a cation, would stick to the sheath surface plugging the pores but would be easily removed by ethanol decolorization. This view supports our Gram staining data, which show gram positivity only at the filament ends. We therefore suggest that the archaeobacterium *M. hungatei* has a unique and characteristic staining response. It depends entirely on the permeability of the end plugs, which are porous to the free diffusion of the staining reagents. These diffuse from the ends toward the filament middle and form crystal violet-iodine or -TPt precipitates which stain the terminal cells purple.

In concert, our data suggest that the plugs are more permeable than the sheath in which they reside. Our concept of diffusible solutes for *M. hungatei* is unique to the procaryotic world; those with an M_r less than 50 (e.g., H_2, CO_2, and CH_4) can pass freely through the sheath, whereas larger solutes must enter through the plugs at the filament ends. Capillary action and microstreaming should enhance the diffusion of solutes along the filament length. In support of this view, small nonionic detergents such as Triton X-100 (a *p-tert*-octylphenlpolyoxyethane; $M_r \approx 633$ [11]) can enter only through the terminal ends, dissolving the cell membranes as they diffuse along the filament (8).

This concept has important consequences for the metabolism and growth of the bacterium. Large endogenous molecules exported by cells within the sheath could diffuse only along the filament length, which may make cell-cell interaction easier, and presumably this could be how terminal flagella are coordinated (18). All cells within the filament should have easy access to small metabolites necessary for cellular growth (CO_2, H_2, NH_3, H_2S, PO_4, etc.), and waste products such as CH_4 should be easily exchanged; the sheath is permeable to them. Yet larger molecules necessary in small quantities for growth, such as vitamins or cofactors, would be required to enter through the end plugs and diffuse along the filament. At the same time, larger organic toxins or lytic enzymes would also require this mode of entry and would therefore affect the terminal cells only until the proper cellular defenses were established. Since flagella are located only at the filament ends (18), one reaction to these chemical stimuli may be to move the cell toward (e.g., vitamins) or away from (e.g., toxins) the reagent. The permeability phenomenon and a tumble-swim mode of locomotion could be used to align cells to chemical gradients and may be a primitive form of taxis.

It is apparent that *M. hungatei* with its unusual style of enveloping its cells within a sheath and plugs had not only shape and form in mind (1). Each enveloping structure has a distinct porosity toward environmental solutes. These attributes make this microorganism a life form that is highly suited to its natural environment; even the strongest armor must have some gaps within it so that certain substances can get in or out. It is possible that other archaeobacteria with complex surface structures may also have atypical Gram reactions.

ACKNOWLEDGMENTS

We acknowledge the able assistance of G. Southam, University of Guelph, for growing some cultures for Gram stains and for fruitful discussions.

This research was supported by a Medical Research Council of Canada operating grant to T.J.B. The electron microscopy was performed in the NSERC Guelph Regional STEM Facility, which is partially supported by an infrastructure grant to T.J.B. from the Natural Sciences and Engineering Research Council of Canada.

REFERENCES

1. **Beveridge, T. J.** 1988. The bacterial surface: general considerations towards design and function. Can. J. Microbiol. **34**:363–372.
2. **Beveridge, T. J.** 1990. Mechanism of Gram variability in select bacteria. J. Bacteriol. **172**:1609–1620.
3. **Beveridge, T. J., and J. A. Davies.** 1983. Cellular responses of *Bacillus subtilis* and *Escherichia coli* to the Gram stain. J. Bacteriol. **156**:846–858.
4. **Beveridge, T. J., R. J. Harris, and G. D. Sprott.** 1987. Septation and filament splitting in *Methanospirillum hungatei*. Can. J. Microbiol. **33**:896–904.
5. **Beveridge, T. J., G. B. Patel, R. J. Harris, and G. D. Sprott.** 1986. The ultrastructure of *Methanothrix concilii*, a mesophilic aceticlastic methanogen. Can. J. Microbiol. **32**:703–710.
6. **Beveridge, T. J., M. Sára, D. Pum, G. D. Sprott, M. Stewart, and U. B. Sleytr.** 1988. Structure, chemistry and physicochemistry of the *Methanospirillum hungatei* GP1 sheath, p. 26–30. *In* U. B. Sleytr, P. Messner, D. Pum, and M. Sára (ed.), Crystalline bacterial cell surface layers. Springer-Verlag KG, Berlin.
7. **Beveridge, T. J., G. Southam, M. H. Jericho, and B. L. Blackford.** 1990. High resolution topography of the S-layer sheath of the archaebacterium *Methanospirillum hungatei* provided by scanning tunneling microscopy. J. Bacteriol. **172**:6589–6595.
8. **Beveridge, T. J., and G. D. Sprott.** Unpublished data.
9. **Beveridge, T. J., M. Stewart, R. J. Doyle, and G. D. Sprott.** 1985. Unusual stability of the *Methanospirillum hungatei* sheath. J. Bacteriol. **162**:728–737.
10. **Davies, J. A., G. K. Anderson, T. J. Beveridge, and H. C. Clark.** 1983. Chemical mechanism of the Gram stain and synthesis of a new electron-opaque marker for electron microscopy which replaces the iodine mordant of the stain. J. Bacteriol. **156**: 837–845.
11. **Helenius, A., D. R. McCaslin, E. Fries, and C. Tanford.** 1979. Properties of detergents. Methods Enzymol. **56**:734–749.
12. **Jarrell, K. F., and S. F. Koval.** 1989. Ultrastructure and biochemistry of *Methanococcus voltae*. Crit. Rev. Microbiol. **17**: 53–87.
13. **König, H.** 1988. Archaeobacterial cell envelopes. Can. J. Microbiol. **34**:395–406.
14. **König, H., R. Kralik, and O. Kandler.** 1982. Structure and modifications of pseudomurein in Methanobacteriales. Zentralbl. Bakteriol. Parasitenkd. Infektionskr. Hyg. Abt. 1 Orig. Reihe C **3**:179–191.
15. **Patel, G. B., L. A. Roth, and G. D. Sprott.** 1979. Factors influencing filament length of *Methanospirillum hungatei*. J. Gen. Microbiol. **112**:411–415.
16. **Salton, M. R. J.** 1963. The relationship between the nature of the cell wall and the Gram stain. J. Gen. Microbiol. **30**:223–235.
17. **Shaw, P. J., G. J. Hills, J. A. Henwood, J. E. Harris, and D. B. Archer.** 1985. Three-dimensional architecture of the cell sheath and septa of *Methanospirillum hungatei*. J. Bacteriol. **161**:750–757.
18. **Southam, G., M. L. Kalmokoff, K. F. Jarrell, S. F. Koval, and T. J. Beveridge.** 1990. Isolation, characterization, and cellular insertion of the flagella from two strains of the archaebacterium *Methanospirillum hungatei*. J. Bacteriol. **172**:3221–3228.
19. **Sprott, G. D., K. M. Shaw, and K. F. Jarrell.** 1983. Isolation and chemical composition of the cytoplasmic membrane of the archaebacterium *Methanospirillum hungatei*. J. Biol. Chem. **258**:4026–4031.
20. **Stewart, M., T. J. Beveridge, and G. D. Sprott.** 1985. Crystalline order to high resolution in the sheath of *Methanospirillum hungatei*: a cross-beta structure. J. Mol. Biol. **183**:509–515.
21. **Yang, L. L., and A. Haug.** 1979. Purification and partial characterization of a procaryotic glycoprotein from the plasma membrane of *Thermoplasma acidophilum*. Biochim. Biophys. Acta **556**:265–277.